

**This is a self-archived version of an original article. This version may differ from the original in pagination and typographic details.**

**Author(s):** Herzberg, R.-D.; Amzal, N.; Becker, F.; Butler, P. A.; Chewter, A. J. C.; Cocks, J. F. C.; Dorvaux, Olivier; Eskola, K.; Gerl, J.; Greenlees, Paul; Hammond, N. J.; Hauschild, K.; Helariutta, Kerttuli; Heßberger, F.; Houry, M.; Jones, G. D.; Jones, Peter; Julin, Rauno; Juutinen, Sakari; Kankaanpää, Harri; Kettunen, Heikki; Khoo, T. L.; Korten, W.; Kuusiniemi, Pasi; Coz, Y. Le; Leino, Matti; Lister, C. J.; Lucas, R.; ...

**Title:** Spectroscopy of transfermium nuclei: No-252(102)

**Year:** 2001

**Version:** Published version

**Copyright:** © 2001, The American Physical Society

**Rights:** In Copyright

**Rights url:** <http://rightsstatements.org/page/InC/1.0/?language=en>

**Please cite the original version:**

Herzberg, R.-D., Amzal, N., Becker, F., Butler, P. A., Chewter, A. J. C., Cocks, J. F. C., Dorvaux, O., Eskola, K., Gerl, J., Greenlees, P., Hammond, N. J., Hauschild, K., Helariutta, K., Heßberger, F., Houry, M., Jones, G. D., Jones, P., Julin, R., Juutinen, S., . . . Wollersheim, H. J. (2001). Spectroscopy of transfermium nuclei: No-252(102). *Physical Review C*, 65(1), Article 014303. <https://doi.org/10.1103/PhysRevC.65.014303>

Spectroscopy of transfermium nuclei:  $^{252}_{102}\text{No}$ 

R.-D. Herzberg,<sup>1</sup> N. Amzal,<sup>1</sup> F. Becker,<sup>2,\*</sup> P. A. Butler,<sup>1</sup> A. J. C. Chewter,<sup>1</sup> J. F. C. Cocks,<sup>3</sup> O. Dorvaux,<sup>3,†</sup> K. Eskola,<sup>4</sup> J. Gerl,<sup>5</sup> P. T. Greenlees,<sup>3</sup> N. J. Hammond,<sup>1</sup> K. Hauschild,<sup>2</sup> K. Helariutta,<sup>3,5</sup> F. Heßberger,<sup>5</sup> M. Houry,<sup>2,‡</sup> G. D. Jones,<sup>1</sup> P. M. Jones,<sup>3</sup> R. Julin,<sup>3</sup> S. Juutinen,<sup>3</sup> H. Kankaanpää,<sup>3</sup> H. Kettunen,<sup>3</sup> T. L. Khoo,<sup>6</sup> W. Korten,<sup>2</sup> P. Kuusiniemi,<sup>3</sup> Y. Le Coz,<sup>2</sup> M. Leino,<sup>3</sup> C. J. Lister,<sup>6</sup> R. Lucas,<sup>2</sup> M. Muikku,<sup>3,§</sup> P. Nieminen,<sup>3</sup> R. D. Page,<sup>1</sup> P. Rahkila,<sup>3</sup> P. Reiter,<sup>7</sup> Ch. Schlegel,<sup>5</sup> C. Scholey,<sup>1</sup> O. Stezowski,<sup>1,||</sup> Ch. Theisen,<sup>2</sup> W. H. Trzaska,<sup>3</sup> J. Uusitalo,<sup>3</sup> and H. J. Wollersheim<sup>5</sup>

<sup>1</sup>Oliver Lodge Laboratory, University of Liverpool, Liverpool L69 7ZE, United Kingdom

<sup>2</sup>DAPNIA/SPhN CEA-Saclay, F-91191 Gif-sur-Yvette Cedex, France

<sup>3</sup>Department of Physics, University of Jyväskylä, Jyväskylä, Finland

<sup>4</sup>University of Helsinki, Helsinki, Finland

<sup>5</sup>Gesellschaft für Schwerionenforschung, Darmstadt, Germany

<sup>6</sup>Argonne National Laboratory, Argonne, Illinois

<sup>7</sup>Ludwig Maximilians Universität, München, Germany

(Received 20 July 2001; published 3 December 2001)

An in-beam study of excited states in the transfermium nucleus  $^{252}\text{No}$  has been performed using the recoil separator RITU together with the JUROSPHERE II array at the University of Jyväskylä. This is the second transfermium nucleus studied in an in-beam experiment. Levels up to spin 20 were populated and compared to levels in  $^{254}\text{No}$ . An upbend is seen at a frequency of 200 keV/ $\hbar$  corresponding to spin 16. We also use an improved systematics to connect the energy of the lowest  $2^+$  state with its half-life and find that the deformation of both  $^{252,254}\text{No}$  is slightly larger than previously assumed.

DOI: 10.1103/PhysRevC.65.014303

PACS number(s): 21.10.-k, 23.20.Lv, 27.90.+b

## I. INTRODUCTION

Nuclei far from stability are an important testing ground for the predictive power of nuclear models. One region of ongoing interest is the transfermium region with its goal being the discovery of a spherical superheavy nucleus with a mass around  $A \approx 300$  [1–4]. While the heaviest nuclei can at present be produced and detected at a rate of a few nuclei per month, the experimental observables mainly yield half-lives,  $\alpha$  decay energies and branching ratios, and production cross sections. These quantities already constrain the parameter space of nuclear structure calculations considerably and are a powerful tool for the study of odd mass nuclei, but today we still cannot distinguish between theoretical predictions for the next spherical shell gap on a purely experimental basis.

Predictions for the structure of a spherical superheavy nucleus range from  $Z = 114$  in the Woods-Saxon model [5] to  $Z = 120$  in relativistic mean field calculations [6] to  $Z = 126$  in Hartree-Fock self-consistent calculations [7]. The recently reported isotopes of elements with  $Z = 114$  [4] and  $Z = 116$  [8] are still on the neutron deficient side for a neutron gap at  $N = 184$ , but approach the  $(Z, N) = (120, 172)$  prediction.

These heaviest systems are produced at the detection

threshold with production cross sections around 1 pb and the possibility of performing any kind of spectroscopy with these nuclei and obtaining detailed level schemes will not be achieved for many years. However, modern techniques such as recoil decay tagging (RDT) [9–11] allow in-beam  $\gamma$  spectroscopic studies on reaction channels as weak as a few hundred nanobarns. The usefulness of this technique in the transfermium region has recently been demonstrated in several studies of the  $Z = 102$  nucleus  $^{254}\text{No}$  [12–14]. The production cross section for  $^{254}\text{No}$  in the  $^{208}\text{Pb}(^{48}\text{Ca}, 2n)$  reaction was 2–3  $\mu\text{b}$ , mainly because of the very favorable combination of a doubly magic target and projectile [12,13,15,16].

The region around  $^{254}\text{No}$  is predicted [6,7,17–19] to be well deformed and indeed the available experimental data show that these nuclei exhibit quadrupole deformations of  $\beta_2 \approx 0.25$ –0.3 leading to rotational level schemes. The deformed mean field causes a splitting of the spherical single particle levels from around the predicted spherical gaps and, therefore, gives us a chance to probe these orbitals in this lower mass region.

In this paper we discuss a study of the neighboring nucleus  $^{252}\text{No}$  via the  $^{206}\text{Pb}(^{48}\text{Ca}, 2n)$  reaction with a production cross section of  $\sigma \approx 220$  nb.

## II. EXPERIMENTAL DETAILS

The experiment was carried out using the JUROSPHERE II array coupled to the gas-filled separator RITU at the University of Jyväskylä [11]. This setup has the advantage that the lead target is in the separator gas volume and can thus be stationary while still easily withstanding the thermal load of up to 25 pnA of  $^{48}\text{Ca}$  beam. The targets were made from isotopically highly enriched  $^{206}\text{Pb}$  as self-supporting foils of 500  $\mu\text{g}/\text{cm}^2$ . The beam was produced by the K130 cyclotron

\*Present address: GANIL, F-14021 Caen, France.

†Permanent address: I.R.e.S. Strasbourg, IN2P3-CNRS, F-67037 Strasbourg, France.

‡Present address: CEA/DIF DCRE/SDE/LDN F-91680 Bruyeres-le-Chatel, France.

§Present address: Daresbury Laboratory, Daresbury WA4 4AD, U.K.

||Permanent address: I.P.N. Lyon, IN2P3-CNRS, F-69037 Lyon, France.

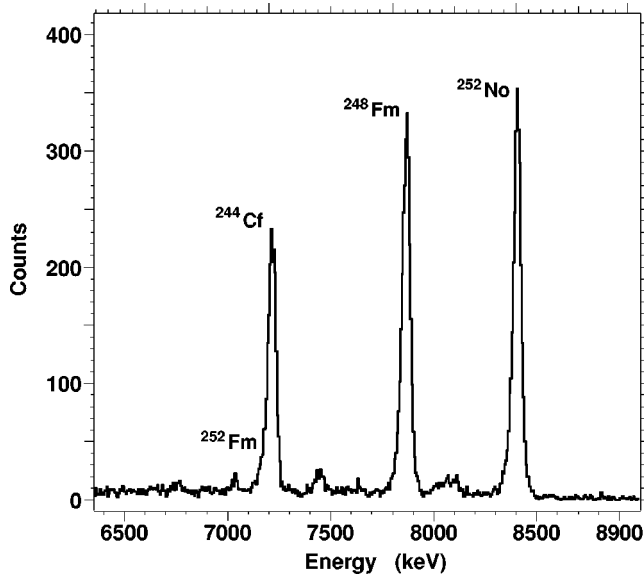


FIG. 1. Total  $\alpha$  decay spectrum in the focal plane of RITU. Only  $^{252}\text{No}$  is produced directly, the peaks labeled  $^{248}\text{Fm}$  and  $^{244}\text{Cf}$  stem from the daughter and granddaughter decays, respectively. The small peak at 7.04 MeV stems from the  $\alpha$  decay of  $^{252}\text{Fm}$  produced via the  $\beta^+$  branch of  $^{252}\text{No}$  and the subsequent  $\epsilon$  decay of  $^{252}\text{Md}$ .

with a laboratory energy of 215.5 MeV at the center of the target. A rough excitation function was performed between 211 MeV and 220 MeV and the energy was chosen 2 MeV above the maximum to enhance the population of higher spin states [14].

During the beamtime a total of  $(9.3 \pm 0.9) \times 10^{16}$   $^{48}\text{Ca}$  nuclei passed through the target and 2800  $\alpha$  decays from the ground state of  $^{252}\text{No}$  were detected at the focal plane of RITU. To estimate the cross section, one has to take into account the various decay branches. In [20] the following values are adopted (a)  $\alpha$ ,  $58 \pm 10\%$ ; (b) fission,  $19 \pm 5\%$ ; and (c)  $\beta^+$ ,  $23 \pm 12\%$ . The  $\beta^+$  branch is based on calculations [21]. If indeed a large  $\beta^+$  branch of  $23 \pm 12\%$  were present, the  $\alpha$  spectrum shown in Fig. 1 should contain a large peak from  $^{252}\text{Fm}$  at 7.04 MeV. The observed peak contains  $45 \pm 15$  events that sets an upper limit to the ratio of  $\beta^+/\alpha = 1.6(5)\%$ . Using the measured ratio  $\alpha/\text{SF} = 75.8/24.2$  [20], we obtain the decay branches of  $^{252}\text{No}$  as (a)  $\alpha$ ,  $74.8 \pm 4\%$ ; (b) fission,  $24 \pm 4\%$ ; and (c)  $\beta^+$ ,  $< 1.6\%$ .

Assuming that only 50% of the  $\alpha$ 's are detected as full energy  $\alpha$ 's and taking into account the relative decay branches given above, this means that  $7500 \pm 400$   $^{252}\text{No}$  nuclei were produced, giving a product of production cross section and separation efficiency of  $\sigma\epsilon \approx (55 \pm 6)$  nb. We give the product  $\sigma\epsilon$  rather than the individual values because of the problems inherent in determining the separator efficiency for these heavy systems precisely. Assuming a RITU efficiency of 25% gives a cross section  $\sigma = (220 \pm 25)$  nb in rough agreement with the cross sections found in the literature [22,23].

$\gamma$  rays were detected in the JUROSPHERE II array consisting of 27 Compton suppressed HPGe detectors (15 Eurogam Phase I, 5 Nordball, 7 Tessa) with a total photopeak efficiency of 1.7%. The beam current used was limited by the

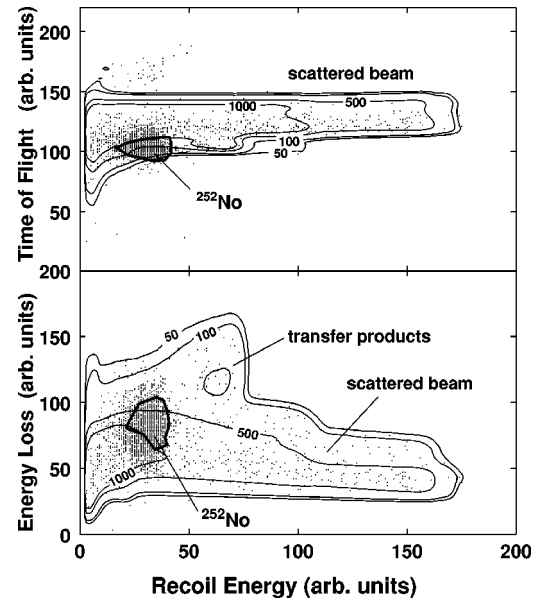


FIG. 2. Top: Time of flight versus recoil energy. Bottom: Energy loss in the MWPC versus recoil energy. The dots show the  $^{252}\text{No}$  nuclei identified by their  $\alpha$  decay. The contour lines show the distribution of all recorded recoil events in the RITU focal plane. The thick contours show the positions of the final gates for  $^{252}\text{No}$ .

count rate in the detectors in the forward direction, which was kept below 11 kHz.

$\gamma$  rays from  $^{252}\text{No}$  were identified in two ways. First we exploited the fact that the  $2n$  evaporation channel is the only fusion-evaporation channel open in this reaction and a  $\gamma$ -recoil coincidence was used. Here the identification of the recoiling  $^{252}\text{No}$  nuclei was greatly helped by the introduction of a multiwire proportional counter (MWPC) 10 cm in front of the position sensitive focal plane Si implantation detector. Using the energy loss signal in the MWPC ( $dE$ ) in conjunction with the full energy signal in the implantation detector ( $E$ ) and the observed time of flight (TOF) between the MWPC and the implantation detector a clean identification of the  $^{252}\text{No}$  evaporation residues was possible and  $\gamma$  ray spectra could be recorded. This is illustrated in Fig. 2 where two of the three projections of the  $E$ - $dE$ -TOF cube on the  $E$ - $dE$ , the  $E$ -TOF, and the TOF- $dE$  planes are shown. The contour lines show the location of all recoil events stemming mainly from scattered beam particles and transfer products, while the dots show those events that are accompanied by a subsequent characteristic  $^{252}\text{No}$   $\alpha$  decay. The plot also allows an estimate of the number of random correlations in this data set. Setting various gates on the recoil distribution in this three dimensional parameter space allows the peak to background ratio to be optimized in the coincident  $\gamma$  spectra. The top and middle panels of Fig. 3 show two examples of  $\gamma$  spectra obtained with wide and optimized gates as indicated in Fig. 2. Although the statistics suffer from the narrower gates, it is clear that the higher transitions especially (above 400 keV) can be identified much better.

Second, an unambiguous identification of the observed  $\gamma$  rays on an event-by-event basis was performed using the recoil decay tagging method [10]. As each recoil is im-

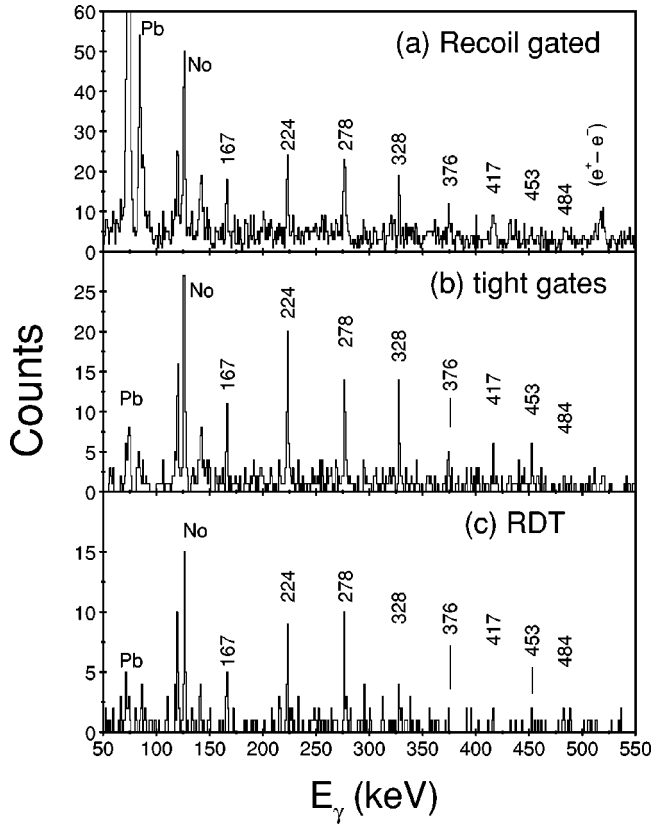


FIG. 3. Top: All  $\gamma$  rays in coincidence with a  $^{252}\text{No}$  recoil nucleus. Middle: Only those  $\gamma$  rays where the recoil passes the gates indicated in Fig. 2. Bottom:  $\gamma$  rays identified through a subsequent  $\alpha$  decay within three half-lives of the  $^{252}\text{No}$  recoil.

planted into the position sensitive implantation detector all  $\gamma$  rays in coincidence are stored. If a  $^{252}\text{No}$   $\alpha$  decay is observed within three half-lives after the implant at the same position of the implantation detector, the recoil is identified and the  $\gamma$  rays are incremented into an RDT spectrum shown in the bottom panel of Fig. 3. Considering that the fission branch reduced the  $\alpha$  decay probability, this procedure served only to uniquely identify the  $\gamma$  rays observed in the recoil gated spectra. No peaks were found in the recoil gated spectra that did not belong to  $^{252}\text{No}$  and therefore all subsequent data analysis was performed with the recoil gated spectra only.

The setup also allowed the tagging of recoils by detecting a fission event within a suitable time interval after the recoil implant. The results of this procedure will be reported elsewhere.

### III. RESULTS

The half-life of  $^{252}\text{No}$  could be determined from the time difference between the implanted recoil and the subsequent  $\alpha$  decay. Since there is a finite probability of a second recoil being implanted in the same pixel before the previously implanted recoil has decayed, a background component with a half-life corresponding to the average implantation rate per pixel has to be taken into account when determining the  $^{252}\text{No}$  half-life. The true lifetime  $\tau$  is obtained from the two apparent components  $\tau_{\text{short}}$  and  $\tau_{\text{random}}$  via  $\tau^{-1} = \tau_{\text{short}}^{-1}$

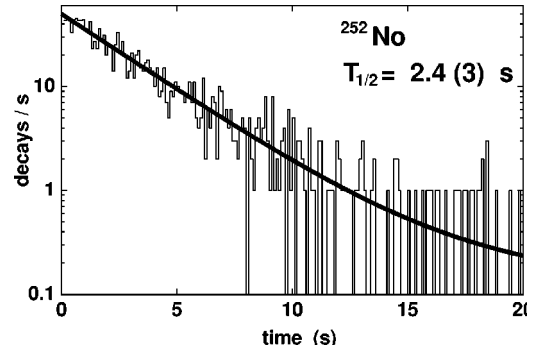


FIG. 4. The  $\alpha$  decay of  $^{252}\text{No}$ . Indicated are the two components of the decay curve. The resulting half-life is  $T_{1/2} = 2.4(3)$  s (see text).

$-\tau_{\text{random}}^{-1}$ . In Fig. 4 the decay curve is shown together with a double exponential fit employing the procedure given by Bartsch *et al.* [24], yielding the half-life of  $^{252}\text{No}$  as  $T_{1/2} = (2.4 \pm 0.3)$  s consistent with the previous values of  $T_{1/2} = (2.25^{+0.18}_{-0.16})$  s [15],  $T_{1/2} = (2.4^{+0.5}_{-0.4})$  s [23],  $T_{1/2} = (2.3 \pm 0.2)$  s [25], and  $T_{1/2} = (2.4 \pm 0.2)$  s [26].

From the  $\gamma$  spectra we observe a rotational structure very similar to that found in  $^{254}\text{No}$ . In these heavy systems the total conversion coefficient for  $E2$  transitions is considerable, falling below unity only at transition energies above 220 keV. However, a Harris fit to the lowest six visible  $\gamma$  rays allows an extrapolation to the lower transition energies according to the prescriptions given in [27–29]. This procedure gives good fits only for one choice of spins with the 167-keV  $\gamma$  ray stemming from the  $6^+ \rightarrow 4^+$   $E2$  transition. We therefore give the spin assignments without parentheses, even though no direct measurement of the multiplicities involved was possible. In the fit procedure the transitions in the up-bend region above the  $12^+$  level were excluded and Harris parameters  $J_0 = 64.45\hbar^2/\text{MeV}$  and  $J_1 = 206.9\hbar^2/\text{MeV}^3$  were obtained.

Assuming no direct feeding to the  $6^+$  state one can compare the intensity ratio  $I(8^+ \rightarrow 6^+)/I(6^+ \rightarrow 4^+)$  to the predictions assuming either  $E2$  or  $E1$  character for both transitions. The experimental ratio is  $I(8^+ \rightarrow 6^+)/I(6^+ \rightarrow 4^+) = 1.8 \pm 0.7$  that must be compared to the expected values  $I(8^+ \rightarrow 6^+)/I(6^+ \rightarrow 4^+) = 2.1$  for  $E2$  transitions and  $I(8^+ \rightarrow 6^+)/I(6^+ \rightarrow 4^+) = 0.93$  for  $E1$  transitions, favoring the former. The same ratio as for  $E2$  transitions is expected for  $M1$  transitions. However, from the number of recoils passing

TABLE I. Comparison of the expected and observed intensities for the two transitions at 167 keV and 224 keV given as a function of the internal conversion coefficient for the indicated multiplicities. The electric quadrupole character is favored.

$\pi\lambda$	167 keV	224 keV
$M1$	$11 \pm 1$	$18 \pm 2$
$E1$	$131 \pm 15$	$119 \pm 14$
$E2$	$37 \pm 4$	$64 \pm 8$
Expt.	$26 \pm 6$	$44 \pm 8$

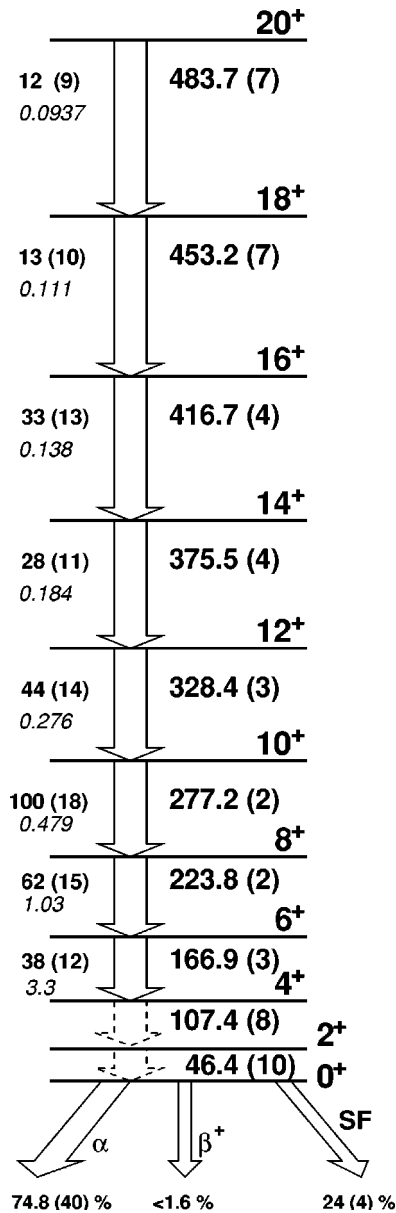


FIG. 5. Level scheme of  $^{252}\text{No}$ . The numbers on the left hand side of a transition indicate the relative intensity of the  $\gamma$  transition, the number in italics below it gives the internal conversion coefficient. The spin labels are given without parentheses, although no spin has been measured directly. See the discussion in the text.

the gates, the absolute efficiency of the JUROSPHERE array, the conversion coefficients, and the relative population of the states (from [14]) for the 167 keV and 224 keV transitions one finds that the assignment of  $E2$  is strongly favored (see Table I).

Figure 5 shows the level scheme obtained from the observed transitions. The dashed transitions are from the extrapolation only. The two numbers given are the observed  $\gamma$  intensity normalized to the intensity of the  $10^+ \rightarrow 8^+$  transition and the total conversion coefficient for the transition assuming  $E2$  character for all transitions (in italics) [30].

The highest transitions are visible at the statistical limit, but combining the information from the recoil tagged spectra

TABLE II. Summary of the transition energies observed for  $^{252}\text{No}$  (This work, [38]) and  $^{254}\text{No}$  ([12–14]).

$J_i \rightarrow J_f$	$^{252}\text{No}$	$^{254}\text{No}$
$2^+ \rightarrow 0^+$ <sup>a</sup>	46.4(10)	44.0
$4^+ \rightarrow 2^+$ <sup>a</sup>	107.4(8)	102.0
$6^+ \rightarrow 4^+$	166.9(3)	158.9
$8^+ \rightarrow 6^+$	223.8(2)	214.1
$10^+ \rightarrow 8^+$	277.2(2)	267.2
$12^+ \rightarrow 10^+$	328.4(3)	318.2
$14^+ \rightarrow 12^+$	375.5(4)	366.5
$16^+ \rightarrow 14^+$	416.7(4)	413
$18^+ \rightarrow 16^+$	453.2(7)	456
$20^+ \rightarrow 18^+$	483.7(7)	498

<sup>a</sup>Energy not measured, but extrapolated from Harris fit.

and the RDT gives reasonable confidence in these transitions. Any higher lying transition will be difficult to populate as the cross section drops rapidly as the energy is further increased.

#### IV. DISCUSSION

The experimental data shows that the nucleus  $^{252}\text{No}$  is a well deformed nucleus with a well defined rotational level sequence. It is now interesting to compare the level scheme to that of  $^{254}\text{No}$ . Table II summarizes all data on level energies available for both nuclei and shows how similar these nuclei are. The dynamic moments of inertia plotted for both nuclei in Fig. 6 show that  $^{252}\text{No}$  shows signs of an upbend around  $\omega \approx 200 \text{ keV}/\hbar$ , while the behavior of  $^{254}\text{No}$  is much smoother. This is illustrated much more clearly in the bottom

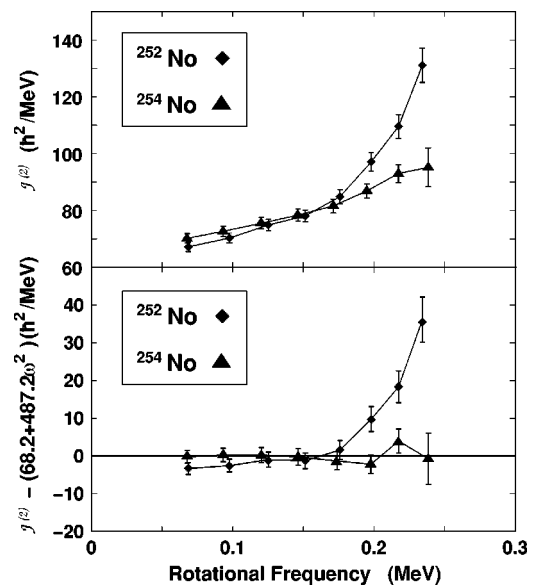


FIG. 6. Top: The moments of inertia for  $^{252}\text{No}$  (squares) and  $^{254}\text{No}$  (triangles). Bottom: The same, but a smooth Harris reference has been subtracted from both moments of inertia. While starting out very similarly, the  $^{252}\text{No}$  nucleus seems to create an upbend around a frequency of 200  $\text{keV}/\hbar$  corresponding roughly to spin 16.

half of Fig. 6, where the dynamic moments of inertia are plotted with the smooth Harris reference subtracted.

This behavior can be reproduced by calculations using the Hartree-Fock-Bogolyubov method with Lipkin-Nogami approximate particle projection [31] where the influence of volume and surface pairing is investigated in detail. There it is found that the dynamic moments of inertia of  $^{252,254}\text{No}$  are very similar at low frequencies. At frequencies above 200 keV/ $\hbar$  the dynamic moment of inertia of  $^{252}\text{No}$  increases more strongly than that of  $^{254}\text{No}$  in qualitative agreement with the experimental data.

It is possible to derive a quadrupole deformation from the extrapolated  $2^+ \rightarrow 0^+$  transition energy from the prescriptions of Grodzins [32] and Raman [33]. However, these global formulas have to be treated with caution in this mass region if they are to give anything more than a rough idea of the deformations involved. The uncertainties especially have to be estimated very carefully, as the parameters entering the fit are usually highly correlated. Unfortunately, these correlation matrices are not given in [33]. We therefore plotted the available data from the ENSDF database on half-lives for 247  $2^+$  states in even-even nuclei with masses  $A > 56$  versus the different approaches and get an estimate for the scatter of the datapoints at the high mass end of the distribution. We also fitted the distribution of all suitable data included in the NUDAT database available at the BNL [34]. The three global approaches are ‘‘Grodzins,’’

$$\tau_\gamma = (2.74 \pm 0.91) \times 10^{13} E^{-4} Z^{-2} A; \quad (1)$$

‘‘Raman’s best fit,’’

$$\tau_\gamma = (1.25 \pm 0.50) \times 10^{14} E^{-(4.00 \pm 0.03)} Z^{-2} A^{(0.69 \pm 0.05)}; \quad (2)$$

‘‘This work,’’

$$\tau_\gamma = (2.9 \pm 1.5) \times 10^{12} E^{-(3.807 \pm 0.023)} Z^{-2} A^{(1.237 \pm 0.065)}. \quad (3)$$

The energies are in keV and the lifetimes in picoseconds. All three global approaches give the lifetime to within 30%. This gives an uncertainty for the quadrupole deformation of roughly 15%.

The actinide nuclei lie on a somewhat different trajectory from the lower mass nuclei. We therefore also performed a local fit to just 23 nuclei with mass  $A > 200$  and  $E(2^+_1) < 150$  keV. This resulted in a much reduced scatter of the data for this region, but must be regarded as nothing more than a local parameter fit to the data,

$$\begin{aligned} \text{‘‘Local fit,’’ } \ln(\tau_\gamma Z^2) &= (65.15 \pm 4.22) \\ &- (4.017 \pm 0.111) \ln(E) \\ &- (5.23 \pm 0.70) \ln(A). \end{aligned} \quad (4)$$

The correlation matrix for the parameters is given in Table III and clearly shows that the correlations are extremely important in this case. Within the range of the fit, the overall uncertainty of the lifetime is 14% giving an uncertainty for  $\beta_2$  of 7%. Figure 7 shows the relevant data points together

TABLE III. Correlation matrix for the local fit (Eq. 4)  $\ln(\tau_\gamma Z^2) = a + b \ln(E) + c \ln(A)$  with  $a = 65.15 \pm 4.22$ ,  $b = -4.017 \pm 0.111$ ,  $c = -5.23 \pm 0.70$  using  $\tau$  in ps and  $E$  in keV.

	$a$	$b$	$c$
$a$	1.000	-0.874	-0.998
$b$	-0.874	1.000	0.846
$c$	-0.998	0.846	1.000

with the fit.

It must be noted, that in the Cf and Cm nuclei where Coulomb excitation studies are available [35], the level energies are of the order 43 keV, and the measured  $B(E2) \uparrow$  are around  $15 e^2 b^2$  giving quadrupole deformations of  $\beta_2 \approx 0.3$ . Taking the extrapolated energies for  $^{252,254}\text{No}$ ,  $E_{2^+}^{252} = 46.4 \pm 1.0$  keV and  $E_{2^+}^{254} = 44.2 \pm 0.4$  keV, we get deformation parameters  $\beta_2^{252} = 0.28 \pm 0.02$  and  $\beta_2^{254} = 0.29 \pm 0.02$ . These values are slightly higher than the value  $\beta_2^{254} = 0.27 \pm 0.02$  given in [12,13], but there the global fits were used. In the light of the global fit performed in this work, even the uncertainty of that value seems to be underestimated by a factor of 2.

The trend predicted from this data is that  $^{252}\text{No}$  should be slightly less deformed than  $^{254}\text{No}$ , simply because the energy of its lowest  $2^+$  state is somewhat higher than that of  $^{254}\text{No}$ . Any other conclusions are marred by the large uncertainties involved in getting a lifetime from a systematic approach. Direct lifetime measurements using Coulomb excitation in inverse kinematics are highly desirable for all nuclei in this region.

Interesting systematics have been given by Zamfir *et al.* [36], who plot the  $B(E2; 2^+ \rightarrow 0^+)_Q$  values of heavy nuclei against the product  $N_p N_n$ . The quantity  $N_p N_n$  is the product of valence particles or holes and is, therefore, sensitive to the location of the next spherical shell gap and the subscript  $Q$  indicates that the effects of hexadecapole deformation have been removed from the data [36],

$$B(E2; 2^+ \rightarrow 0^+)_Q = B(E2; 2^+ \rightarrow 0^+) \left( \frac{Q(\beta_4 = 0)}{Q(\beta_4 \neq 0)} \right)^2.$$

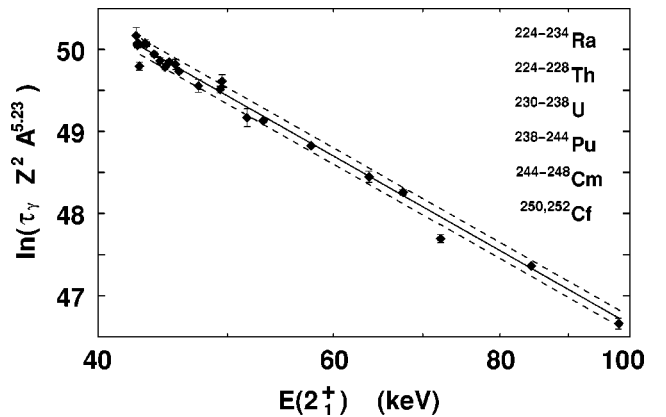


FIG. 7. Experimental lifetimes (measured in ps) versus excitation energy. The dashed lines show the uncertainty of the fit (Eq. 4).

TABLE IV. Transition energies in keV and reduced transition probabilities in W.u. for the lowest  $2^+$  states in  $^{252,254}\text{No}$ . For the definition of  $B(E2; 2^+ \rightarrow 0^+)_Q$  see the explanation in the text.

	$E(2^+)$	$B(E2; 2^+ \rightarrow 0^+)$	$B(E2; 2^+ \rightarrow 0^+)_Q$
$^{252}\text{No}$	$46.4 \pm 1.0$	$390 \pm 50$	$370 \pm 50$
$^{254}\text{No}$	$44.0 \pm 1.0$	$420 \pm 50$	$410 \pm 50$

This correction is also applied to the  $B(E2)$  values for  $^{252,254}\text{No}$  but using the deformation parameters of both Möller *et al.* [19] and Sobiczewski *et al.* [37] they are smaller than 5% for  $^{252}\text{No}$  and 2% for  $^{254}\text{No}$ , respectively. This is much less than the uncertainties due to the extrapolation procedure that are around 12%, see Table IV.

Assuming a shell gap to be either at  $(Z, N) = (114, 184)$ ,  $(Z, N) = (120, 172)$  or at  $(Z, N) = (126, 184)$ , the values  $N_p N_n$  for  $^{252,254}\text{No}$  are quite different. In Fig. 8 the systematics is shown together with the  $B(E2)_Q$  values for both nobelium isotopes using either  $(Z, N) = (114, 184)$  (closed circles),  $(Z, N) = (120, 172)$  (open triangles) or  $(Z, N) = (126, 184)$  (open circles) as the next shell gap. The errorbars are still fairly large and the uncertainties involved in such a procedure preclude definitive statements.

An in-beam  $\gamma$  spectroscopic study of the transfermium nucleus  $^{252}\text{No}$  has been performed. The ground state rotational band was observed up to spin  $20\hbar$ . From a Harris fit the energy of the highly converted  $2^+ \rightarrow 0^+$  transition was determined as  $46.4(10)$  keV. This is somewhat higher than the corresponding transition energy in  $^{254}\text{No}$ . A careful reexamination of the systematic dependence of the lifetime of the  $2_1^+$  state on its energy for very heavy nuclei has led to a revised quadrupole deformation of  $\beta_2^{252} = 0.31 \pm 0.02$  and  $\beta_2^{254} = 0.32 \pm 0.02$  at variance with earlier estimates using the global systematics of  $\beta_2^{254} = 0.27 \pm 0.02$ . The ground state band of  $^{252}\text{No}$  shows an upbend at a frequency of  $\omega \approx 200$  keV/ $\hbar$  that is absent in  $^{254}\text{No}$ . Further experiments aimed at the observation of the lowest two transitions in

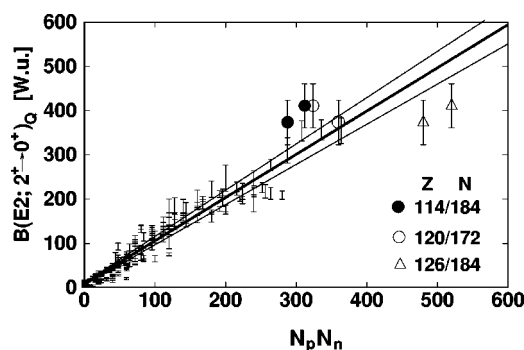


FIG. 8. Experimental  $B(E2; 2^+ \rightarrow 0^+)_Q$  values versus the product  $N_p N_n$ . The values obtained for  $^{252,254}\text{No}$  are indicated assuming the next spherical shell gap at  $(Z, N) = (114, 184)$  (closed circles),  $(Z, N) = (120, 172)$  (open triangles) or  $(Z, N) = (126, 184)$  (open circles), respectively. The figure is reproduced from [36].

conversion electron spectroscopy are highly desirable to establish the low energy part of the level scheme and plan for the future.

#### ACKNOWLEDGMENTS

We would wish to thank the accelerator staff at the University of Jyväskylä for their efforts in providing a high quality beam. We also acknowledge valuable discussions with R. Bengtsson and are grateful to P. Bonche and T. Duguet for sharing their calculations prior to publication. We are also grateful to N.V. Zamfir for many valuable discussions and permission to use Fig. 8 here. This work was supported by the Access to Large Scale Facility program under the Training and Mobility of Researchers program of the European Union, the Access to Large Scale Facility program under the TMR program of the EU (Contract No. ERBFMGECT950037), the Academy of Finland under the Finnish Center of Excellence Program 2000–2005 (Project No. 44875), the U.K. Engineering and Physical Sciences Research Council, and the U.S. Department of Energy (Contract No. W-31-109-ENG-38). R.D.H. acknowledges support by EPSRC.

- [1] P. Armbruster, Rep. Prog. Phys. **62**, 465 (1999).  
 [2] S. Hofmann, Rep. Prog. Phys. **61**, 639 (1998).  
 [3] G. Münzenberg, Rep. Prog. Phys. **51**, 57 (1988).  
 [4] Y. T. Oganessian *et al.*, Nature (London) **400**, 242 (1999).  
 [5] S. Cwiok *et al.*, Nucl. Phys. **A573**, 356 (1994).  
 [6] K. Rutz *et al.*, Phys. Rev. C **56**, 238 (1997).  
 [7] S. Cwiok *et al.*, Nucl. Phys. **A611**, 211 (1996).  
 [8] Y. T. Oganessian *et al.*, Phys. Rev. C **63**, 011301(R) (2001).  
 [9] K.-H. Schmidt *et al.*, Lect. Notes Phys. **219**, 244 (1984); K.-H. Schmidt *et al.*, Phys. Lett. **168B**, 39 (1986).  
 [10] E. S. Paul *et al.*, Phys. Rev. C **51**, 78 (1995).  
 [11] M. Leino *et al.*, Nucl. Instrum. Methods Phys. Res. B **99**, 653 (1995).  
 [12] P. Reiter *et al.*, Phys. Rev. Lett. **82**, 509 (1999).  
 [13] M. Leino *et al.*, Eur. Phys. J. A **6**, 1 (1999).  
 [14] P. Reiter *et al.*, Phys. Rev. Lett. **84**, 3542 (2000).  
 [15] Yu. A. Lazarev *et al.*, Phys. Scr. **39**, 422 (1989).  
 [16] H. W. Gäggeler *et al.*, Nucl. Phys. **A520**, 641c (1989).  
 [17] Z. Patyk and A. Sobiczewski, Nucl. Phys. **A533**, 132 (1991).  
 [18] S. Cwiok *et al.*, Nucl. Phys. **A573**, 356 (1994).  
 [19] P. Möller *et al.*, At. Data Nucl. Data Tables **59**, 185 (1995).  
 [20] Y. A. Akaoli, Nucl. Data Sheets **84**, 1 (1998).  
 [21] P. Möller, J. R. Nix, and K.-L. Kratz, At. Data Nucl. Data Tables **66**, 131 (1997).  
 [22] G. N. Flerov, Y. T. Oganessian, A. A. Pleve, N. V. Pronin, and Y. P. Tretyakov, Nucl. Phys. **A267**, 359 (1976).  
 [23] F. P. Hessberger *et al.*, J. Less-Common Met. **122**, 445 (1986); F. P. Hessberger, GSI Report GSI-85-11, 1985.  
 [24] H. Bartsch *et al.*, Nucl. Instrum. Methods **121**, 185 (1974).  
 [25] C. E. Bemis *et al.*, Phys. Rev. C **15**, 705 (1977).  
 [26] Y. T. Oganessian, Sov. J. At. Energy **28**, 502 (1970).  
 [27] J. E. Draper *et al.*, Phys. Rev. C **42**, R1791 (1990).

- [28] J. Becker *et al.*, Phys. Rev. C **46**, 889 (1992).
- [29] G. Hackman *et al.*, Phys. Rev. Lett. **79**, 4100 (1997).
- [30] F. Rösel *et al.*, At. Data Nucl. Data Tables **21**, 292 (1978).
- [31] T. Duguet, P. Bonche, and P.-H. Heenen, Nucl. Phys. **A679**, 427 (2001).
- [32] L. Grodzins, Phys. Lett. **2**, 88 (1962).
- [33] S. Raman *et al.*, At. Data Nucl. Data Tables **42**, 1 (1989).
- [34] R. R. Kinsey *et al.*, The NUDAT/PCNUDAT Program for Nuclear Data, paper submitted to the 9th International Symposium on Capture Gamma-Rays and Related Topics, Budapest, Hungary, 1996. Data extracted from the NUDAT database, version 23/2/2000 at the NNDC.
- [35] *Table of Isotopes*, 8th ed., edited by R. B. Firestone and V. S. Shirley (Wiley, New York, 1996).
- [36] N. V. Zamfir *et al.*, Phys. Lett. B **357**, 515 (1995).
- [37] A. Sobczewski *et al.*, Phys. Rev. C **63**, 034306 (2001).
- [38] R.-D. Herzberg *et al.*, in *Proceedings of the Second International Conference on Fission and Properties of Neutron Rich Nuclei*, edited by J. H. Hamilton, W. R. Phillips, and H. K. Carter (St. Andrews, Scotland, 1999), p. 196.